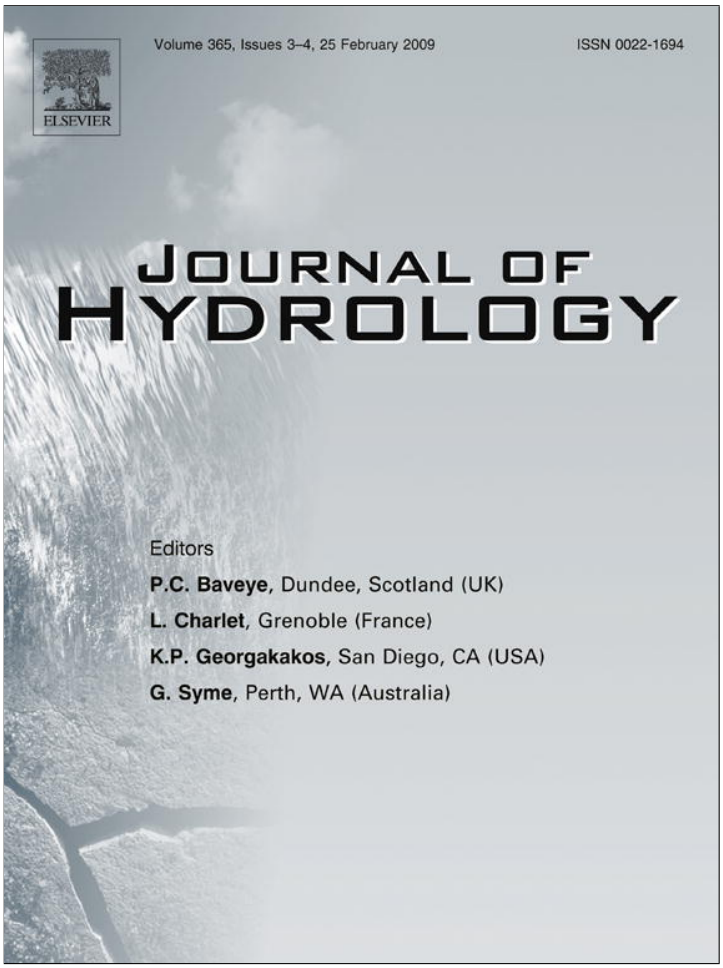

Journal of Hydrology 365 (2009) 289–301

Contents lists available at ScienceDirect

Journal of Hydrology

journal homepage: www.elsevier.com/locate/jhydrol

Associations of interdecadal/interannual climate variability and long-term colorado river basin streamflow

Janak Timilsena [a], Thomas Piechota [b,*], Glenn Tootle [c], Ashok Singh [d]

[a] PBS&J, 2270 Corporate Circle, Suite 100, Henderson, NV 89074-7755, United States
[b] Dept. of Civil and Environmental Engineering, University of Nevada, Las Vegas, 4505 Maryland Parkway, Box 454015, Las Vegas, NV 89154-4015, United States
[c] Department of Civil and Environmental Engineering, University of Tennessee, 223 Perkins Hall, Knoxville, TN 37996-2010, United States
[d] Hotel Management, University of Nevada, Las Vegas, 4505 Maryland Parkway, Box 454020, Las Vegas, NV 89154-4020, United States

ARTICLE INFO

Article history:
Received 17 November 2007
Received in revised form 20 November 2008
Accepted 26 November 2008

Keywords:
Interdecadal
Interannual
Climate variability
Streamflow
ENSO
PDO
AMO
Reconstruction

SUMMARY

The study presented here utilized long-term streamflow records (over 500 years) to investigate the influence of interannual/interdecadal climate variability on the Colorado River basin. 19 unimpaired water year streamflow stations were reconstructed utilizing partial least square regression using standard tree ring chronologies. The spatial and temporal variability of drought was evaluated for all the stations for the different centuries in the record. Finally, the relationship between individual impact of ENSO, PDO, and AMO and its combined effect on streamflow was determined using the non parametric Rank Sum test for different lag years (0, +1, +2, and +3) of streamflow. This research also determined the change in streamflow volume with respect to the long-term mean volume of the basin due to individual and coupled effect of oceanic climate influences. Results indicate that there is an increase in streamflow during El Niño and decreased streamflow during La Niña in the basin. Similarly, PDO warm/cold resulted in increased/decreased streamflow. There were few stations related to the AMO in the basin. Finally, the differences in the Upper and Lower basin were noted in the magnitude of changes in streamflow (in terms of percentage) under different individual and coupled influences of ENSO, PDO, and AMO.

Published by Elsevier B.V.

Introduction

Reconstructed data of hydrologic variables such as streamflow, precipitation and palmer drought severity index (PDSI) are important for the study of climate variability (e.g., Cook et al., 1999,2004; Hidalgo et al., 2000; Gray et al., 2004; Woodhouse et al., 2006). Longer records using paleoclimatic data (e.g., tree-rings) are necessary to understand the magnitude of past droughts and to develop improved understanding of interannual and interdecadal phenomenon (ENSO, PDO, AMO, and NAO). To date, studies that have investigated interannual and interdecadal variability in streamflow have used instrumental data from 50 to 100 years (e.g. Piechota and Dracup, 1996; Cayan et al., 1999; Gershunov and Barnett, 1998; Dettinger and Diaz, 2000; Enfield et al., 2001; Sutton and Hudson, 2005; Tootle et al., 2005; Hunter et al., 2006 and McCabe et al., 2007). The limitation of using instrumental data is that phenomena such as the PDO and AMO persist for 20–50 years and the instrumental record would only cover one to two phases. The use of reconstructed streamflow data is an opportunity for improved understanding of how regional hydrology is influenced by interannual and interdecadal phenomenon. Explanation of the interannual and interdecadal variability in streamflow has been attributed to oceanic–atmospheric phenomenon such as the PDO, AMO, and ENSO. Shorter term variability is best explained by evaluation of the relevant hydrologic parameters (e.g., precipitation, soil moisture) that are drivers of streamflow.

There are a variety of methods available to reconstruct hydroclimatic variables from tree-ring data. Stahle et al.(1998a,b), Touchan et al. (1999), Diaz et al. (2001), Woodhouse (2001), and Gray et al. (2004) used multiple linear regression and stepwise multiple linear regression to reconstruct hydroclimate variables such a precipitation, streamflow and other drought variables. Similarly, Stockton and Jacoby (1976), Cook and Jacoby (1983), Garen (1992), Meko et al. (2001), Hidalgo et al. (2000), and Woodhouse et al. (2006) used principal component regression for streamflow reconstruction.

Another method available for reconstruction of hydroclimate data is partial least square regression (PLSR) which was developed in the late 1960s (Wold, 1966) and gained importance in the field of chemistry during the 1970s (Gerlach et al., 1979). PLSR has recently been used for reconstruction of summer temperatures in eastern Norway (Kalela-Brundin, 1999). PLSR generalizes and combines features from principal component regression and multiple linear regressions (Ablitt et al., 2004).

* Corresponding author. Tel.: +1 702 895 4412.
E-mail addresses: jtimilsena@pbsj.com (J. Timilsena), thomas.piechota@unlv.edu (T. Piechota), gtootle@utk.edu (G. Tootle), aksingh@unlv.nevada.edu (A. Singh).

0022-1694/$ - see front matter Published by Elsevier B.V.
doi:10.1016/j.jhydrol.2008.11.035

There is a high level of uncertainty associated with these reconstructions of streamflow data and climatic–oceanic phenomenon. This may be due to due to unknown biological factors (e.g., disease in the trees), natural or manmade occurs such as wildland fires, and the presence of long-term climate change. However, the reconstructions are still able to capture the high-frequency climate variability which is the focus of this study. Additional inclusion of low-frequency proxies (predictors) such as lake sediments would help to integrate the low-frequency climate variability (Moberg et al., 2005).

The objective and contribution of this research was to utilize reconstructed streamflow time series for the evaluation of individual and coupled impact of ENSO, PDO, and AMO on streamflow of the Colorado River basin. The investigation of the impact of ENSO, PDO, and AMO, and its combined effect on streamflow is significant since no studies have been performed using long-term reconstructed streamflow records. This will provide comprehensive and valuable information about the impact of high and low frequency ocean climate phenomena in this region. Further, the reconstruction of 19 streamflow stations in the Colorado River basin is significant since past studies have focused on a limited number of stations in the basin.

Data sources

Unimpaired streamflow data

In reconstructing long-term hydroclimate variability, it is important to use unimpaired streamflow data which provides an account of hydrologic responses to fluctuations in climate for watershed (Slack and Landwehr, 1993). Unimpaired streamflow stations for the Upper and Lower Colorado River basin were obtained from the United States Geological Survey (USGS), Hydro-Climate Data Network (HCDN) (http://pubs.usgs.gov/wri/wri934076/1st_page.html) and the Bureau of Reclamation (Reclamation) (http://www.usbr.gov/lc/region/g4000/NaturalFlow/current.html) natural flow data. In the upper basin, there were 14 stations which had at least 50 years of regular unimpaired streamflow record, a sufficient number of overlapping years with tree ring data, and at least four predictors (tree ring sites) that were highly correlated ($r > 0.5$) with the streamflow station. Out of these 14 stations, 11 stations data were based on HCDN, and three stations (Yampa River near Maybell, Green River at Greendale, and San Juan River near Bluff) unimpaired data were based on natural flow data of the Colorado River Basin (http://www.usbr.gov/lc/region/g4000/NaturalFlow/current.html). Similarly in the Lower basin, there were five (5) sites which met the above criteria out of which four stations were from HCDN and one station (Virgin River at Littlefield) was from the natural flow data of the Colorado River Basin (http://www.usbr.gov/lc/region/g4000/NaturalFlow/current.html) (see Table 1 and Fig. 1).

Tree-ring data

Tree-ring data were compiled from the International Tree Data Bank (http://www.ncdc.noaa.gov/paleo/treering.html) maintained by the National Oceanic and Atmospheric Administration (NOAA), World Data Center for Paleoclimatology. Tree-ring data consisted of information on tree species, standard normal width, standard residual width, and wood density measurement with its location. The standard normal widths of site chronologies (hereinafter referred to as standard tree-ring chronologies) represent the growth indices for each site, and this information was used for the unimpaired streamflow reconstructions. Altogether, the Upper Colorado River basin includes 57 standard tree-ring chronologies; and the Lower Colorado basin contains 54, of which 35 in the Upper and seven (7) in the Lower have at least 500 years of record. These 42 standard tree-ring chronologies are shown in Fig. 1 and were utilized as predictors for the calibration and reconstruction of unimpaired streamflow stations (Table 2). These 42 standard tree-ring chronologies were selected based on their available data over the last 500 years and sufficient overlapping period with the streamflow stations. Of these 42 standard tree-species, 19 were Douglas Fir, 11 were Pinyon species (PIED), four were Ponderosa pine (PIPO), three were Spruce species(PCEN), and two were Limber pine (PIFL). The remaining three were Great basin BC pine (PILO), White pine (PISF) and Rocky Mountain BC pine (PIAR).

Reconstructed interdecadal and decadal oceanic data

El Niño-southern oscillation (ENSO)

ENSO is a natural coupled cycle in the ocean-atmospheric system over the tropical Pacific that operates on a timescale of 2–7 year (Hanley et al., 2003). The warm phase of ENSO is referred to as the El Niño and the cool phase is defined as the La Niña. The phase and strength of ENSO events are defined by indices; however, there is no single index that best describes the ENSO years and their corresponding strength, timing and duration of events (Hanley et al., 2003). The tree-ring reconstructed average Southern Oscillation Index (SOI) for the month of December/January/Febru-

Table 1
Summary of the unimpaired streamflow stations in the Colorado River basin utilized in this study along with the source of the data.

Station number	Station name	State	Drainage area (Sq. km)	Datum elevation (m)	Data duration (water year)	Source
9112500	East River at Almont	CO	749	2440	1935–2005	HCDN
9119000	Tomichi Creek at Gunnison	CO	2748	2325	1938–2005	HCDN
9124500	Lake Fork at Gateview	CO	865	2386	1938–2005	HCDN
9128500	Smith Fork Near Crawford	CO	111	2161	1936–1988	HCDN
9147500	Uncompahgre River at Colona	CO	1160	1926	1913–2005	HCDN
9239500	Yampa River at Steamboat Springs	CO	1564	2041	1911–2005	HCDN
9251000	Yampa River Near Maybell	CO	8832	1798	1917–2005	HCDN
9299500	Whiterocks River Near Whiterocks	UT	293	2182	1930–2005	Reclamation
9304500	White River Near Meeker	CO	1955	1920	1910–2005	HCDN
9310500	Fish Creek Above Reservoir Near Scofield	UT	156	2338	1939–2005	HCDN
9361500	Animas River at Durango	CO	1792	1982	1928–2005	HCDN
9364500	Animas River at Farmington	NM	3522	1609	1931–2005	HCDN
9403000	Bright Angel Creek Near Grand Canyon	AZ	262	760	1924–1973	HCDN
9415000	Virgin River at Littlefield	AZ	13,183	538	1930–2005	Reclamation
9430500	Gila River Near Gila	NM	4828	1419	1929–2005	HCDN
9444500	San Francisco River at Clifton	AZ	7164	1047	1936–2005	HCDN
9498500	Salt River Near Roosevelt	AZ	11,153	664	1914–2005	HCDN
9234500	Green River at Greendale	UT	50,097	1705	1906–2004	Reclamation
9379500	San Juan River Near Bluff	UT	59,547	1234	1906–2004	Reclamation

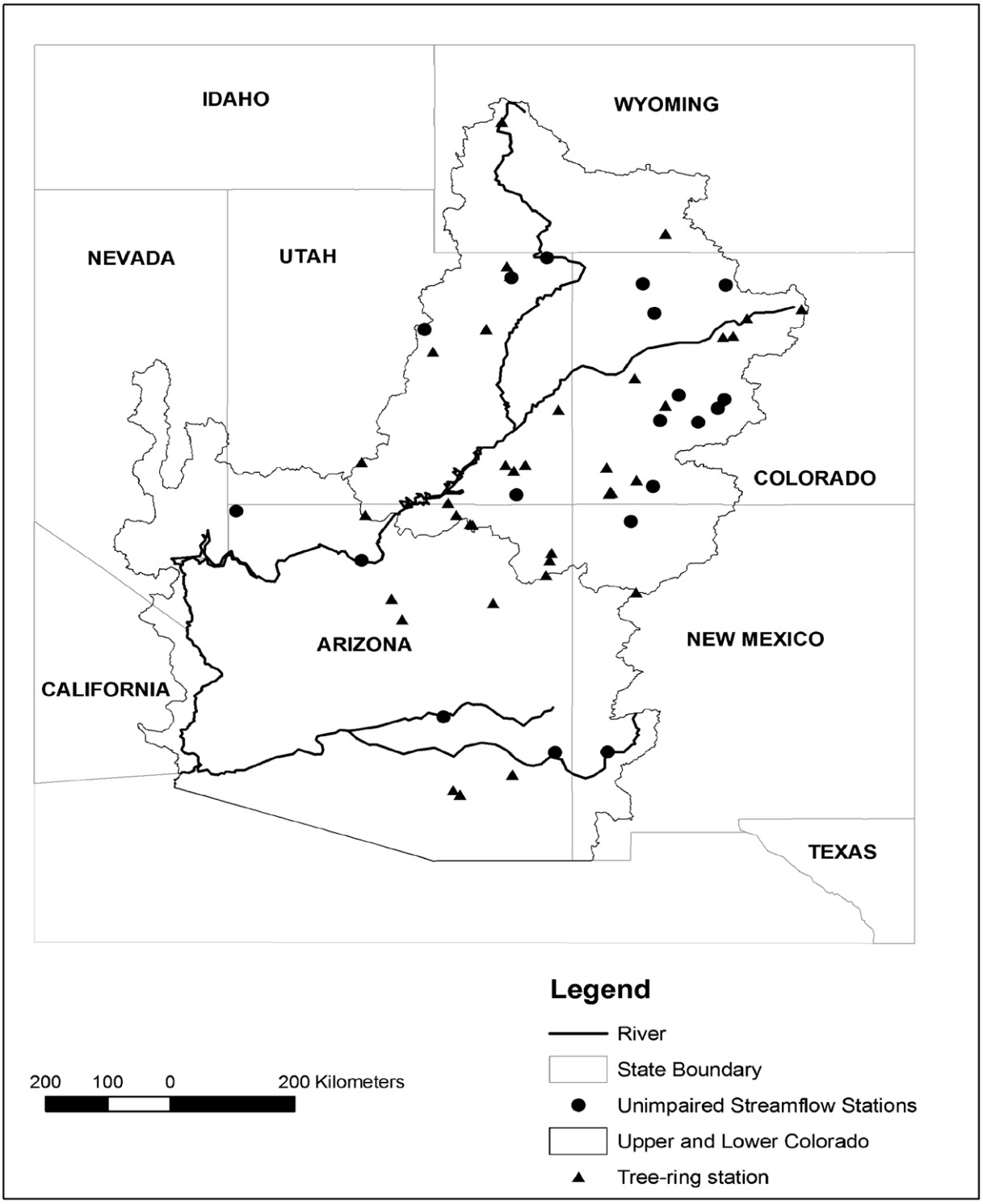

Fig. 1. Location map displaying 19 unimpaired streamflow stations and 42 standard tree-ring chronologies. Unimpaired streamflow stations are indicated by black dark circle. Standard tree-ring chronologies are indicated by the small dark triangles.

ary by Stahle et al. (1998a, b) was utilized from the National Oceanic and Atmospheric Administration (NOAA) Paleoclimatology Program, World Data Center (WDC) for Paleoclimatology website (http://www.ncdc.noaa.gov/paleo/recons.html). Stahle et al. (1998a, b) utilized 14 tree-ring chronologies from northern Mexico (Durango and Chihuahua), the southwestern USA (Arizona, Utah and New Mexico) and Java, Indonesia plus the first two factor scores from a network of 9 chronologies in OK and TX as predictors in reconstructing the SOI. El Niño (warm phase) years were defined as a year with SOI less than −1.0 and La Niña (cold phase) years were defined as a year with SOI greater than 1.0.

Pacific decadal oscillation (PDO)

The Pacific decadal oscillation (PDO) is a long-lived ENSO-like pattern of Pacific climate variability defined as the leading principal component of North Pacific monthly sea surface temperature vari-

Table 2
Summary of the standard tree-ring chronologies utilized in this study.

ITRB site name	Altitude (m)	Tree-ring duration	Tree species
Monarch Lake	2621	1430–1987	Ponderosa Pine (PIPO)
Schulman Old Tree Number 1 Mesa Verde	2103	1400–1963	Douglas Fir (PSME)
Eagle	1951	1107–1964	Douglas Fir (PSME)
Black Canyon of the Gunnison River	2426	1478–1964	Douglas Fir (PSME)
Upper Gunnison	2530	1322–1964	Douglas Fir (PSME)
Eagle East (Job 105 Reworked)	2164	1314–1964	Pinyon Species (PIED)
Dolores	2195	1457–1978	Douglas Fir (PSME)
Dolores	2195	1270–1978	Pinyon Species (PIED)
Satan Pass	2286	1381–1972	Douglas Fir (PSME)
Bobcat Canyon	2042	1390–1971	Douglas Fir (PSME)
Spruce Canyon	2115	1373–1978	Douglas Fir (PSME)
Hogback Rampart Hills	3230	1484–1994	Limber Pine (PIFL)
Pumphouse	2195	1320–1999	Pinyon Species (PIED)
Land's End	2987	1135–2000	Douglas Fir (PSME)
Navajo National Monument	2012	1304–1962	Douglas Fir (PSME)
Defiance West (Defiance/Nazlini)	2134	1474–1965	Douglas Fir (PSME)
Canyon de Chelly	1828	1376–1972	Douglas Fir (PSME)
Tseh-Ya-Kin Canyon	1951	1500–1971	Douglas Fir (PSME)
Betatakin Canyon	2042	1263–1972	Douglas Fir (PSME)
Shonto Plateau	2134	1365–1971	Pinyon Species (PIED)
Tsegi Point Road	2196	1490–1972	Pinyon Species (PIED)
Paria Plateau	1860	1481–1975	Pinyon Species (PIED)
Wind River Mountains Site D	2500	1492–1972	Limber Pine (PIFL)
Medicine Bow Peak	3150	1401–1983	Spruce Species (PCEN)
Unita Mountain	3353	1433–1971	Spruce Species (PCEN)
La Sal Mountains Site A	2323	1489–1972	Pinyon Species (PIED)
Kane Spring	1966	1445–1971	Pinyon Species (PIED)
Navajo Mountain	2286	1469–1971	Pinyon Species (PIED)
White Canyon	1859	1347–1972	Douglas Fir (PSME)
Milk Ranch Point	2286	1276–1970	Pinyon Species (PIED)
Uinta Mountains Site D	2289	1423–1971	Pinyon Species (PIED)
Nine Mine Canyon High	1920	1194–1964	Douglas Fir (PSME)
Nine Mine Canyon	1920	1201–1949	Douglas Fir (PSME)
Water Canyon Bryce Canyon National Park	2098	1336–1964	Ponderosa Pine (PIPO)
Wild Horse Ridge	2805	286–1985	Gt. basin B.C. Pine (PILO)
San Francisco Peaks A	3535	548–1983	Rocky Mtn. B.C. Pin (PIAR)
Green Mountain	2194	1460–1986	Ponderosa Pine (PIPO)
Walnut Canyon	2057	1420–1987	Ponderosa Pine (PIPO)
Fort Grant Overlook Pinaleno Mountains	2896	1249–1991	White Pine (PISF)
Snow Bowl San Francisco Peak	3150	1453–1983	Spruce Species (PCEN)
Reef of Rocks	2550	1321–1998	Douglas Fir (PSME)
Reef of Rocks	3025	1464–1999	Douglas Fir (PSME)

ability (poleward of 20°N for the 1900–1993 periods) (Shen et al., 2006; Mantua et al., 1997). The PDO has two phases: warm and cold which persist for approximately 25 years. The tree-ring data reconstructed PDO (1661–1991) by Biondi et al. (2001) was utilized from the NOAA Paleoclimatology Program and WDC for Paleoclimatology (http://www.ncdc.noaa.gov/paleo/recons.html). Biondi et al. (2001) utilized tree-ring chronologies from Southern California to Sierra San Pedro Martir in northern Baja California situated in a direction roughly parallel to the coastline to reconstruct the PDO.

Atlantic multidecadal oscillation (AMO)

The leading mode of low-frequency, North Atlantic Ocean (0–70°) SST variability with a periodicity of 65–80 years is termed the Atlantic Multidecadal Oscillation (Kerr, 2000; Gray et al, 2004). The AMO has two phases, warm and cold, that persist for about 30–40 years. The tree-ring reconstructed time series of AMO by Gray et al. (2004) was utilized in this study and obtained from the NOAA Paleoclimatology Program and WDC for Paleoclimatology (http://www.ncdc.noaa.gov/paleo/recons.html). Gray et al. (2004) utilized 12 tree-ring records from eastern North America, Western Europe, Scandinavia, and the Middle East in order to reconstruct AMO from 1567 to 1990 AD.

Methods

The methods used in this study included those for prescreening of predictor variables, reconstruction of streamflow, and evaluation of linkages with interannual/interdecadal climate variability.

Prescreening of predictors

Prescreening of the standard tree-ring chronologies was carried out by correlation analysis for an overlapping period of instrumental water year (October–September) streamflow and standard tree-ring chronologies. The streamflow stations have different overlapping periods based on available tree-ring chronologies. Available tree ring chronologies based on the three different ending periods; 1960, 1970 or 1980 were utilized for the calibration depending upon the streamflow in order to have a longer overlapping period. The correlation coefficients between water year streamflow and the selected standard tree-ring chronologies (lag −1, 0, and +1) within the basin were obtained. Chronologies that were positively correlated with station water year streamflow with less than 95% significance were eliminated from the prescreening, and were not used as predictors for the respective streamflow reconstruc-

tion. In order to minimize the effect of autocorrelation caused due to the biological carryover effects of the chronologies from year to year, the lagged form (−1, 0, and +1) of the chronologies of standardized tree ring widths were utilized in the reconstruction model (Fritts, 1976, 1991; Hidalgo et al., 2000).

Reconstruction procedure

Partial least square regression

After the determination of the appropriate predictor variables, a PLSR reconstruction model was developed. As noted earlier, PLSR generalizes and combines features from both principal component analysis (PCA) and multiple linear regression (MLR) (Abdi, 2003). PLSR is especially useful when there is a need to provide a prediction from a very large set of independent (predictors) variables (Abdi, 2003). In PLSR, the principal component scores of both (X) and (Y) are used in lieu of the original data to develop the regression model. PLSR identifies components from (Y) that are also relevant for (X) (Abdi, 2003). The generalization step results in PLSR searching for a set of components (latent vectors) that explains the maximum covariance between (X) and (Y) which is followed by a regression step where the decomposition of (X) is used to predict (Y) (Abdi, 2003). To perform PLSR, several methods are available including the nonlinear iterative partial least squares (NIPALS) approach. NIPALS is advantageous due to calculation speed and simplicity (Wold et al., 1987), if the model has few significant principal components. The NIPALS approach was utilized in this research and a detailed procedure is explained in Tootle et al. (in press).

The prediction residual sum of squares (PRESS) statistic is a cross validation calculation that determines the minimum (optimum) number of components required (Geladi and Kowalski, 1986). The cross-validation consists of removing a row (or multiple rows) from the data matrix and then completing the Eigen analysis on the reduced matrix. Target testing is then performed on the removed rows using the various levels of the abstract factor space and the difference between the target points and the predicted points is calculated (Malinowski, 2002). This process is repeated until every row has been deleted once and the errors in the target fit for each row are summed (Malinowski, 2002). The most popular method to determine the optimal number of latent variables is the PRESS statistic with the minimum value (Malinowski, 2002), which was applied to the current research.

Selection of best predictors using instrumental records

In order to find the best predictors in all the models, cross validation based on the correlation criterion was followed. First, significantly (95%) correlated tree-ring chronologies with water year streamflow for the calibration period were ranked based on their absolute value of correlation. Then, PLSR was run for all the significantly correlated tree-ring chronologies. The procedure was followed by eliminating the least significantly correlated variables until the cross validation standard error (CVSE) was minimized (Michealson, 1987).

In this study, independent testing of model performance utilizing the CVSE criterion based on Garen (1992), Hidalgo et al. (2000) and Timilsena et al. (2007) was utilized in order to evaluate the performance of the model. The CVSE is defined as

$$\mathrm{CVSE} = \sqrt{\frac{\sum \left(y_i - \hat{y}_{(i)}\right)^2}{n-p}} \quad (1)$$

where y_i is the observed streamflow for year i; $\hat{y}_i$ is the fitted response of the ith year computed from the fit with the ith observation removed; n is the number of years in the data set; and p is the number of predictors in the regression equation. The best predictors are the remaining tree-ring chronologies after eliminating the least significantly correlated tree-ring chronologies with the minimum CVSE value.

Reconstruction of unimpaired streamflow

All the 19 unimpaired streamflow stations were reconstructed utilizing PLSR. While reconstructing the water year streamflow for the last 500 years, each water year streamflow was calibrated and reconstructed utilizing the tree-ring chronologies ending in 1960, 1970 or 1980 in order to have a longer overlapping period. There were eight stations (Uncampahgre River at Colona, Yampa River at Steamboats, Yampa River near Maybell, White River near Meeker, Bright Angel Creek near Grand Canyon, Salt River near Roosevelt, Green River at Greendale and San Juan River near Bluff) that were calibrated and reconstructed considering all the tree-ring chronologies ending after 1960. Similarly, six (6) stations (East River at Almont, Whiterocks River near Whiterocks, Animas River at Durango, Animas River at Farmington, Virgin River at Littlefield and Gila River near Gila) were calibrated and reconstructed utilizing the standard tree-ring chronologies ending after 1970. The remaining five stations (Tomichi Creek at Gunnision, Lake Fork at Gateview, Smith Fork near Crawford, Fish Creek near Reservoir and San Franscisco River at Clifton) were calibrated and reconstructed utilizing the tree-ring chronologies ending after 1980. Similar to the procedure mentioned earlier, first the tree-ring chronologies were prescreened based on the correlation criterion (>95% confidence level of positive correlations) during the calibration period. Once the pool of predictors based on the correlation criterion was obtained, predictors were ranked based on their value of correlation. Then PLSR was run eliminating each of the least correlated tree-ring chronologies until the minimum CVSE was obtained. As it was defined earlier, the best model had the lowest CVSE.

The variability between the observed and reconstructed water year streamflows was found different. That made it difficult to adjoin the two time series for the drought and teleconnection study. In order to have a closer fit of the reconstructions with the observed data, reconstructed water year streamflow were rescaled to the observed variance using the same approach followed in Timilsena et al. (2007). This approach helps to eliminate shift of variability between instrumental and reconstructed time series, and the evaluation of the streamflow deficit or surplus with reference to a unique long-term mean (i.e. average of historical and adjusted reconstructed time series).

The spatial and temporal variability of drought was analyzed by dividing the streamflow data into epochal time periods. Drought years were defined as the years that have less than 10 percentile water year flow for the last 500 years. Once the drought years were identified for last 500 years, average drought deficit (sum of drought deficit divided by number of drought years) was obtained for each 100 year period for each streamflow station. Linkages of wet and dry periods with oceanic–climatic phenomeon are presented in the following section.

Linkages between streamflow and oceanic-climate phenomenon

The evaluation of linkages between streamflow and oceanic–climatic phenomenon was performed for two cases (individual and coupled impacts).

Individual impact of ENSO, PDO, and AMO on streamflow

In order to evaluate the lagged response of streamflow to ENSO, PDO, and AMO, 0, +1, +2, and +3 lag year time series of streamflow were used. For instance, lag 0 was defined as the relation between the oceanic climate phenomenon and streamflow in the same year. The lag +1 used the current year of the oceanic climate phenomenon and the next year of streamflow. Similarly, lag +2 and lag +3

used the current year of the oceanic climate phenomenon with the next +2 and +3 year data of streamflow. The study of phases (positive or negative) was also performed for the ENSO, PDO, and AMO for significant (95%) differences in the streamflow medians.

The non-parametric Rank Sum test was used to evaluate the individual impacts of ocean-atmospheric phenomenon on unimpaired water year streamflow. The Rank Sum test assumes that the two data sets are identically distributed and there is no assumption of normality (Maidment, 1993). By applying the Rank Sum test, it was possible to determine the significant median difference in water year streamflow volume comparing cold and warm phases of ENSO, PDO, and AMO.

Each year of warm and cold phases of ENSO, PDO, and AMO were identified. As mentioned earlier, El Niño (warm phase) years were defined as a year which has a value of SOI less than −1.0 and La Niña (cold phase) years were defined as a year which had a value of SOI greater than 1.0. In the case of PDO and AMO, the positive index values were considered as the warm phase and the negative values were considered as the cold phase. Once the years of warm and cold phases of each ocean climate phenomenon were determined, the respective streamflow volume time series for each station were obtained. Streamflow for each phase was evaluated considering the significant (greater than 95%) differences in streamflow medians using the Rank Sum test. The streamflow stations that had a significant difference in medians (e.g., cold vs. warm or warm vs. cold) were considered as the impacted streamflow stations with the respective phase of the ocean climate phenomenon.

Coupled impact of ENSO, PDO, and AMO

This step included the study of the coupled impact of ENSO, PDO, and AMO on individual unimpaired water year streamflow of the basin. ENSO was coupled with the PDO and AMO in order to find whether the interannual high frequency variability during ENSO was enhanced or dampened during the multidecadal oceanic climate phenomenon (PDO or AMO). Similarly, coupling of PDO and AMO was done in order to evaluate the variability during the combined PDO and AMO phases.

An example of the coupling of ENSO and PDO was determined using streamflow volume that coincides with the years PDO cold/El Niño, PDO warm/El Niño, PDO cold/La Niña and PDO warm/La Niña. Then the coupled climate phenomenon was evaluated considering the significant (greater than 95%) differences in streamflow medians of PDO cold/El Niño – PDO warm/El Niño and PDO cold/La Niña – PDO warm/La Niña respectively using the Rank Sum test. This same approach was also utilized for the coupled effect of ENSO with AMO and PDO with AMO.

Shifts in mean of streamflow using reconstructed period of record

In addition to the Rank Sum test, the mean differences (in terms of percentage) of water year streamflow of each station for the periods of specific individual/coupled ocean climate phenomenon with respect to the long-term mean were obtained. The mean of the water year volume during specific individual/coupled phenomenon was obtained by taking the average of water year volume during the period of specific individual/coupled ocean climate phenomenon (e.g. PDO cold/AMO warm, PDO cold/AMO cold, PDO warm/AMO cold, PDO warm/AMO cold). Similarly, the long-term mean was obtained by taking an average of water year volume throughout the period (1706–1970). This mean difference study was determined for the lag zero scenarios. The average increase or decrease in percentage flow for all stations was obtained in order to obtain the basin response for the specific ocean climate phenomenon scenario.

Results

Partial least square reconstruction

There were over 100 available standard tree-ring chronologies (including lag −1, 0, and +1 years) prior to prescreening for streamflow calibration. These chronologies had correlation values ranging from 0.86 to 0.00 with water year streamflow depending upon the station. Based on the prescreening criterion of correlation greater than 95% confidence level with the water year streamflow, the number of standard tree-ring chronologies (predictors) was reduced to between 8 and 40 depending on the streamflow station.

PLSR was used to reconstruct streamflow for all 19 stations. Table 3 summarizes the reconstruction performance statistics of the reconstruction during the calibration and validation period of observed water year data. PLSR performed satisfactorily since the calibration model incorporated greater than 48% of observed variability in all the stations. Fig. 2 presents the annual average and the 10-year moving average of water year streamflow

Table 3
Performance statistics of PLSR reconstruction for all 19 unimpaired streamflow stations in the Colorado River basin. CVSE is the cross-validation standard error in 100∗km^3/water year for streamflow.

Station name	USGS station number	% Variance	CVSE (100 Km^3/year)	Calibration period
East River at Almont	9112500	51.48	6.57	1936–1970
Tomichi Creek at Gunnison	9119000	56.11	4.36	1939–1980
Lake Fork at Gateview	9124500	65.22	3.91	1939–1980
Smith Fork near Crawford	9128500	61.36	0.93	1937–1980
Uncampahgre River at Colona	9147500	72.59	4.82	1914–1960
Yampa River at Steamboat Springs	9239500	67.86	6.53	1912–1960
Yampa River Near Maybell	9251000	68.37	24.97	1916–1960
Whiterocks River Near Whiterocks	9299500	56.52	2.017	1931–1970
White River near Meeker	9304500	64.04	7.86	1911–1960
Fish Creek near Reservoir	9310500	59.30	1.12	1940–1980
Animas River at Durango	9361500	79.17	12.55	1929–1970
Animas River at Farmington	9364500	81.07	13.89	1932–1970
Bright Angel Creek near Grand Canyon	9403000	53.77	1.05	1925–1960
Virgin River at Littlefield	9415000	48.52	7.76	1931–1970
Gila River near Gila	9430500	48.90	5.428	1930–1970
San Francisco River at Clifton	9444500	39.40	13.11	1937–1980
Salt River near Roosevelt	9498500	90.12	39.78	1915–1960
Green River at Greendale	9234500	67.19	39.57	1906–1960
San Juan River near Bluff	9379500	75.66	56.15	1906–1960

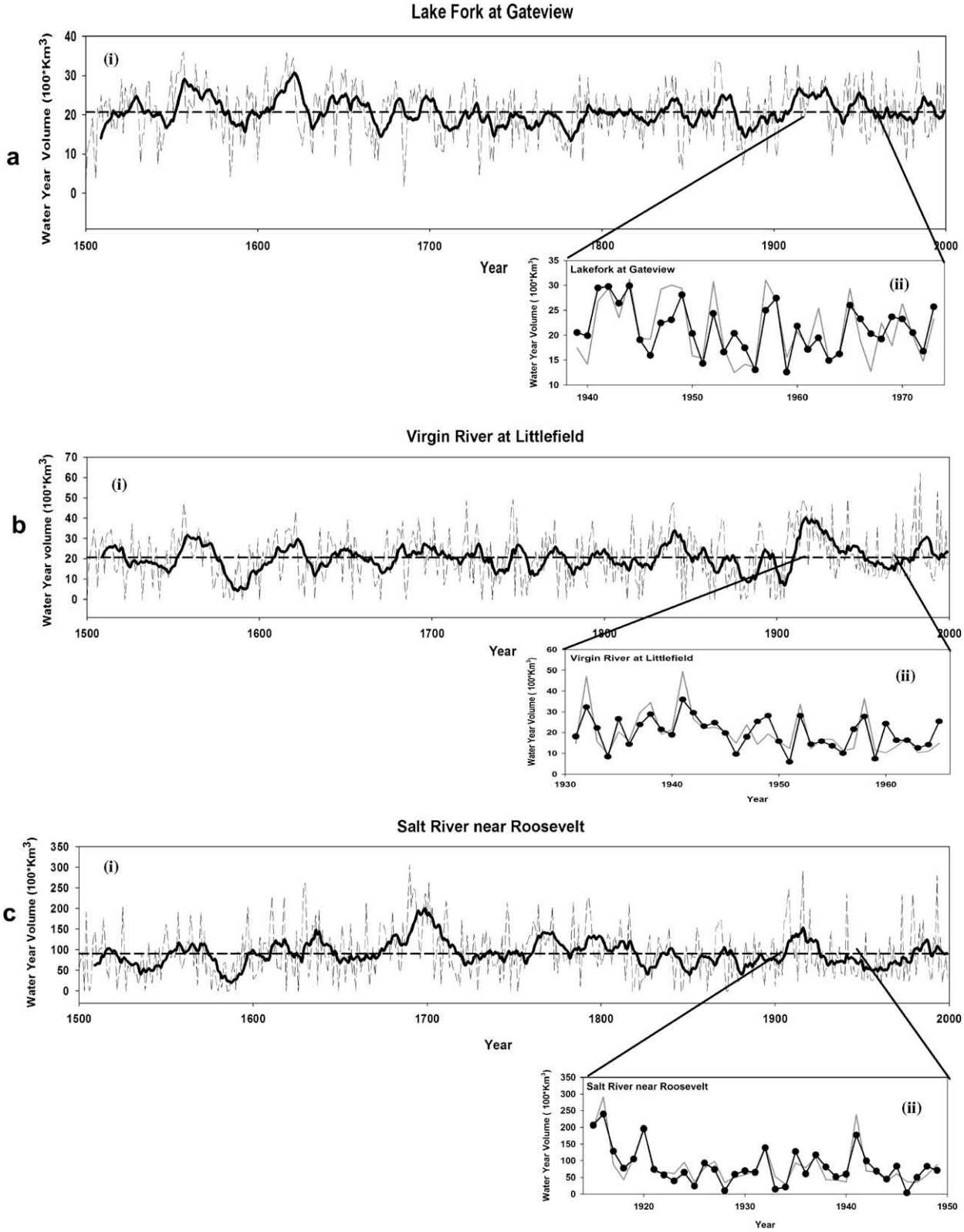

Fig. 2. PLSR reconstructed water year streamflow and calibration ($100*km^3$) representing the annual and 10-year moving average (i) at: (a) lake Fork at Gateview; (b) Virgin river at Littlefield; and (c) salt river near roosevelt white river. The thin short-dashed line indicates the annual water year volume ($100*km^3$). The thick solid line indicates the 10-year moving average. The horizontal medium-dashed line indicates the long-term water year mean. The inserted Figure (ii) represents the calibration comparison of PLSR with observed water year data at: (a) lake Fork at Gateview; (b) Virgin river at Littlefield, and (c) salt river near Roosevelt white river. The solid gray line represents the observed annual water year data. The solid line with circle symbol indicates the PLSR reconstructed water year streamflow ($100*Km^3$).

(adjusted reconstructed plus observed water year streamflow). The three stations presented in Fig. 2 represent the Upper, Middle, and Lower portions of the Basin. Visually inspecting these figures, Fig. 2a has different wet and dry periods than those of Fig. 2b and c. This represents some of the spatial variability in the basin. This is further investigated in Fig. 3a and b.

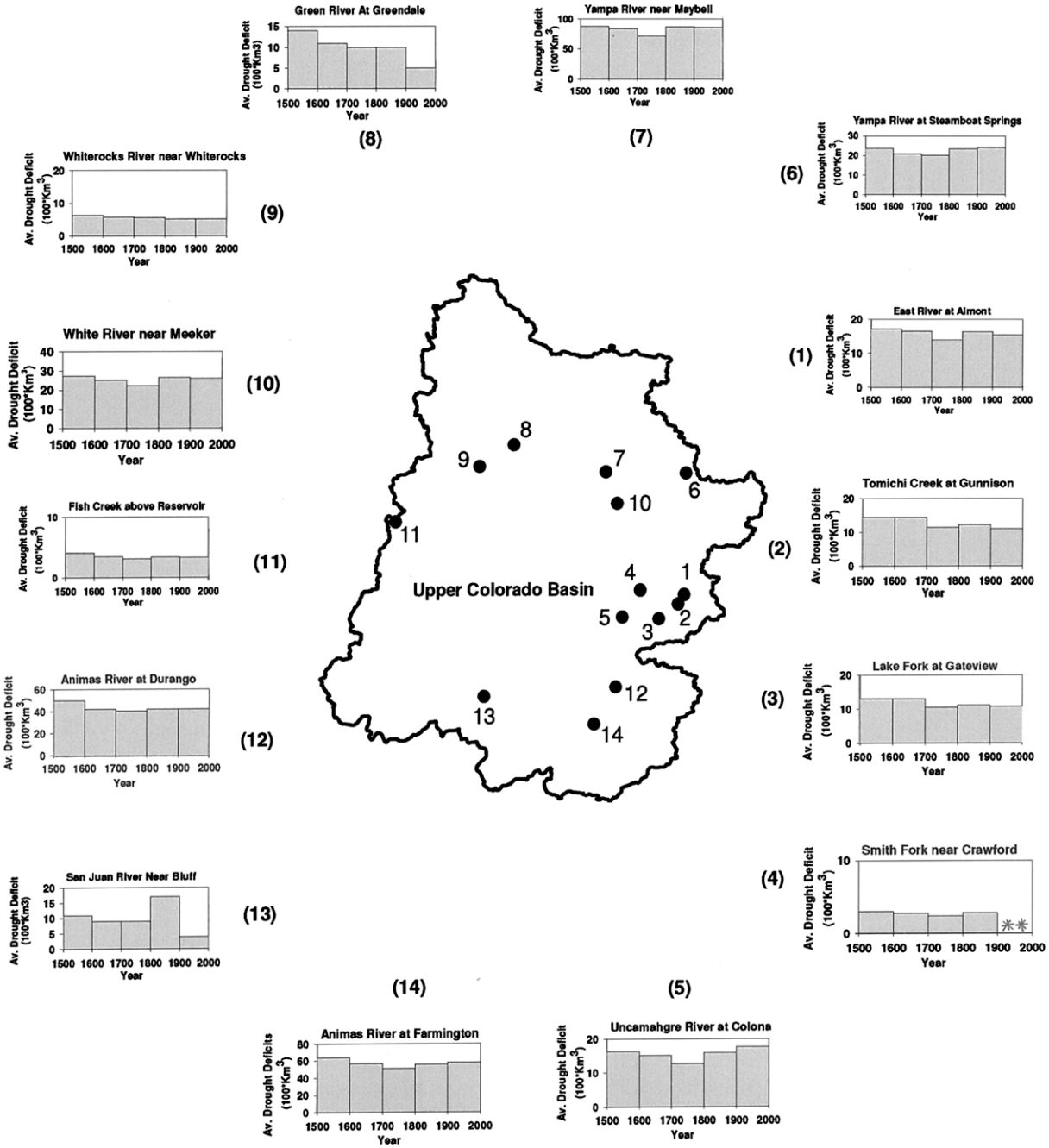

Fig. 3a. Histogram indicating the drought deficit (km^3/year) for each 100 year period (1500–1599, 1600–1699, 1700–1799, 1800–1899, and 1900–1999) for 14 unimpaired streamflow stations in the Upper Colorado basin. The black dark circle indicates the unimpaired streamflow stations in the Colorado river basin. The shaded vertical bar indicates average drought deficit (km^3/year) in each 100 year period. The symbol (**) indicates the 100 year period in which the data were not enough to do the drought analysis.

Fig. 3a summarizes the spatial and temporal variability of the drought deficit based on the adjusted reconstructed plus observed time series of 14 unimpaired streamflow stations in the Upper Colorado River basin. Similarly, Fig. 3b summarizes the spatial and temporal variability of the droughts deficit obtained by the five unimpaired streamflow stations in the Lower Colorado River basin. From the bar diagram, the drought deficit was spatially and temporally varied in the region (upper and lower basin).

Linkages between streamflow and oceanic-climate phenomenon

Individual impact of ENSO, PDO, and AMO

There was a significant (95%) negative difference in medians for 18 out of 19 streamflow stations for the lag 0 year between ENSO cold and ENSO warm. This means that the ENSO cold (La Niña) was associated with decreased streamflow in the region and ENSO warm (El Niño) was associated with increased streamflow. The ENSO relationship with streamflow was not significant

in the lag +1, +2, and +3 years. This result of increased streamflow stations during El Niño (ENSO warm) and decreased streamflow during La Niña (ENSO cold) in the southwest is consistent with previous studies using only historical records by Redmond and Koch (1991), Piechota and Dracup (1996), and Cayan et al. (1999).

The PDO signal was also significant in the streamflow of the Colorado River basin where the PDO warm/cold phase was associated with the increased/decreased streamflow in all 19 streamflow stations. This result was consistent with the Tootle et al. (2005) study that noted increased streamflow in the southwest during the warm phase of PDO. Further, Hunter et al. (2006) also concluded that the decreased SWE in Utah and Colorado was associated with the cold phase of PDO. Since, the PDO is a decadal phenomenon, the lag 0 and lag +1 has similar results, but a decrease in significant stations was observed during the lag +2 and lag +3 year.

The AMO signal was not as clear as compared to PDO and ENSO in the Colorado River basin. There were only four (out of 19) streamflow stations that were associated with the increased/decreased streamflow during the cold/warm phase of AMO. Tootle et al. (2005) and McCabe et al. (2007) also concluded that the low flow generally occurred in the Colorado River basin when the AMO was positive. It is noteworthy that the significant number of stations increased slightly (4–8 out of 19) when the lag was increased from 0 to +1 years but decreased for lag +2 year.

Coupling of interdecadal ENSO, PDO, and AMO

Table 4 presents the six different combinations of coupled ENSO, PDO, and AMO considering the lag 0, +1, +2, and +3 years. The coupling of ENSO with PDO was evaluated for El Niño/PDO cold–El Niño/PDO warm and La Niña/PDO cold–La Niña/PDO warm. Similarly, the ENSO with AMO was evaluated for El Niño/AMO cold–El Niño/AMO warm and La Niña/AMO cold–La Niña/AMO warm. Further, the coupling of PDO and AMO was evaluated for PDO cold/AMO cold–PDO cold/AMO warm and PDO warm/AMO cold–PDO warm/AMO warm.

The coupling of El Niño with PDO (warm/cold) had more streamflow stations impacted in the basin for lag +1 as compared to the individual analysis of ENSO and PDO. This result is consistent with Gershunov and Barnett (1998) who found that the ENSO signal (El Niño/La Niña) was strongest during the different phases of PDO (positive/negative) respectively. In addition, Tootle et al. (2005) and Hunter et al. (2006), found a coupled impact of PDO and ENSO on streamflow. The coupling of ENSO or PDO with AMO resulted in few stations that had significantly different medians. This is consistent with the individual analysis that found a

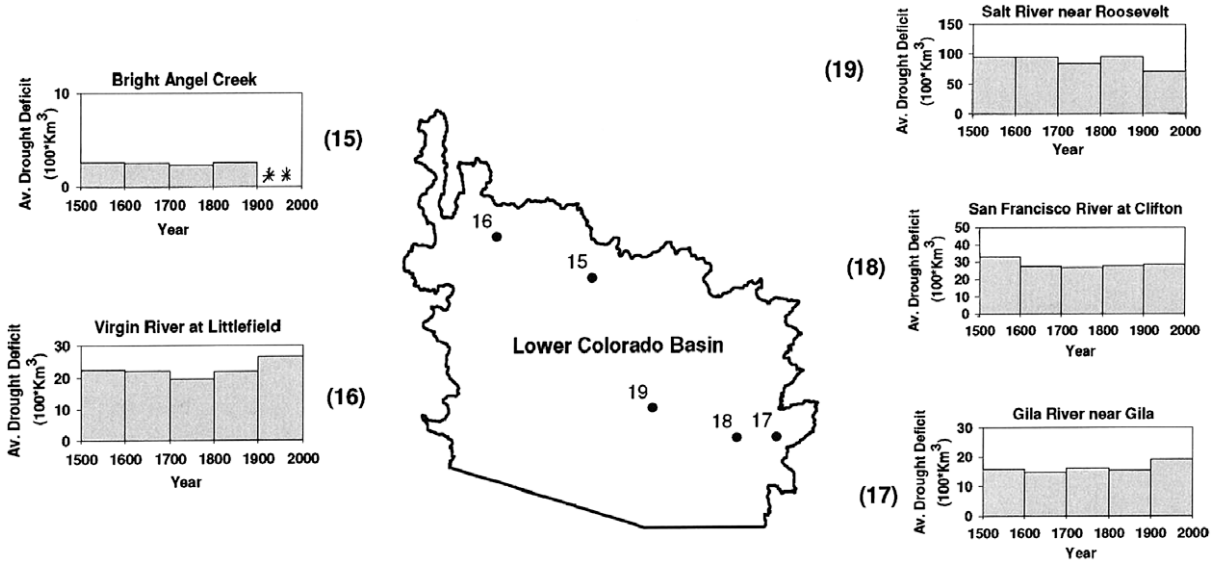

Fig. 3b. Histogram indicating the drought deficit (km^3/year) for each 100 year period (1500–1599, 1600–1699, 1700–1799, 1800–1899, and 1900–1999) for five unimpaired streamflow stations in the Lower Colorado basin. The black dark circle indicates the unimpaired streamflow stations in the Colorado river basin. The shaded vertical bar indicates average drought deficit (km^3/year) in each 100 year period. The symbol (**) indicates the 100 year period in which the data were not enough to do the drought analysis.

Table 4
Coupling impact of ENSO, PDO and AMO on streamflow. The value indicates the number of significant streamflow stations (out of 19 stations) based on the rank sum test under the different scenarios. P and N indicate the positive and negative significant stations, respectively.

	Coupled Phenomenon	Streamflow numbers							
		Lag (0)		Lag (+1)		Lag (+2)		Lag (+3)	
		Nos.	Sign	Nos.	Sign	Nos.	Sign	Nos.	Sign
1	El Niño/PDO cold- El Niño/PDO warm	15	N	17	N	5	N	0	–
2	La Niña/PDO cold- La Niña/PDO warm	13	N	16	N	1	N	0	–
3	El Niño/AMO cold- El Niño/AMO warm	1	P	4	P	1	P	2	P
4	La Niña/AMO cold- La Niña/AMO warm	0	–	3	P	4	P	1	P
5	PDO cold/AMO cold–PDO cold/AMO warm	0	–	0	–	1	P	1	P
6	PDO warm/AMO cold–PDO warm/AMO warm	0	–	0	–	2	P	2	P

weak relationship between AMO and Colorado River basin streamflow.

Shifts in mean of streamflow

The mean differences (in terms of percentage) of water year streamflow for each station for the periods of specific individual/coupled ocean climate phenomenon (18 scenarios) with respect to the long-term mean were obtained. The results are summarized in Fig. 4 where the box represents the distribution of the shift in the mean for all 19 stations in the basin.

In Fig. 4, the largest shifts occurred during El Niño (ENSO warm) and PDO warm (+ 22%) and largest negative shifts during La Niña and PDO cold (−30%). This result was consistent with the Gershunov and Barnett (1998) who found that El Niño impacts were strongest (wettest) during the positive (warm) phase of PDO.

During the AMO warm there was decreased streamflow in the region as compared to AMO cold. When AMO was coupled with PDO, the shifts looked similar to that expected during the PDO warm and cold phases alone. Similarly, when AMO was coupled with El Niño and La Niña, the shifts were similar to that expected

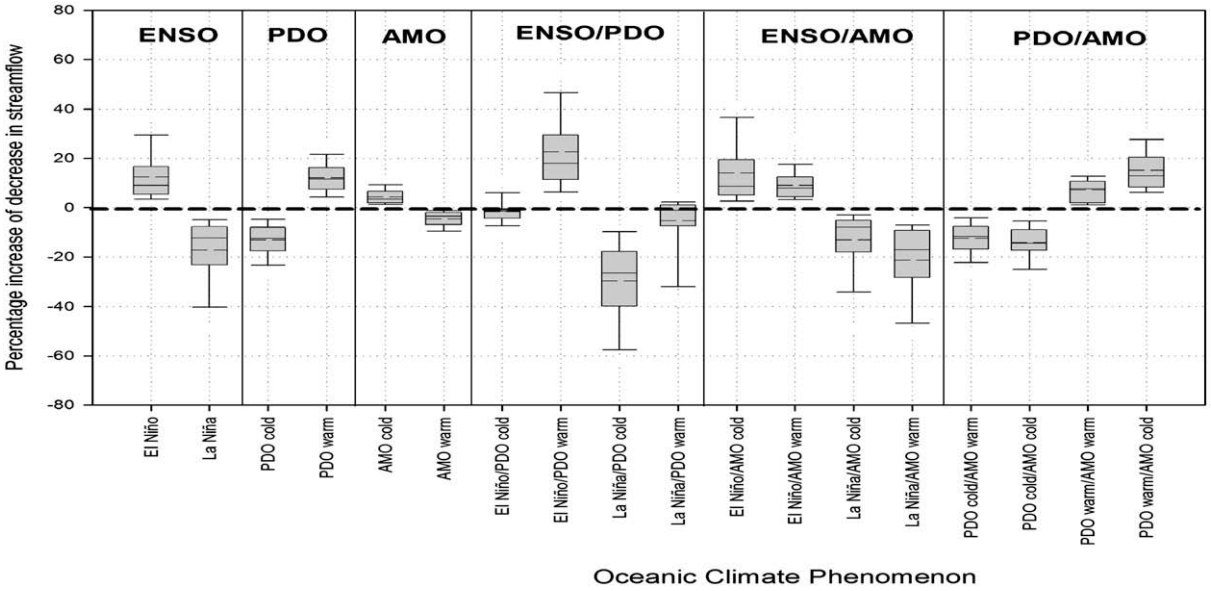

Fig. 4. Box and Whisker plots that shows mean, median, and percentile (5th, 25th, 75th, and 95th) increase/decrease (in terms of percentage) in streamflow volume (considering all 19 stations) due to individual and coupling effect of oceanic climate phenomenon. The box delineates the 25th and 75th percentile. Whiskers are the 5th and 95th percentile. The horizontal dash line inside the box indicates mean. The horizontal bold straight line inside the box indicates the median. The long horizontal dot line indicates the line of zero percentage of increase or decrease.

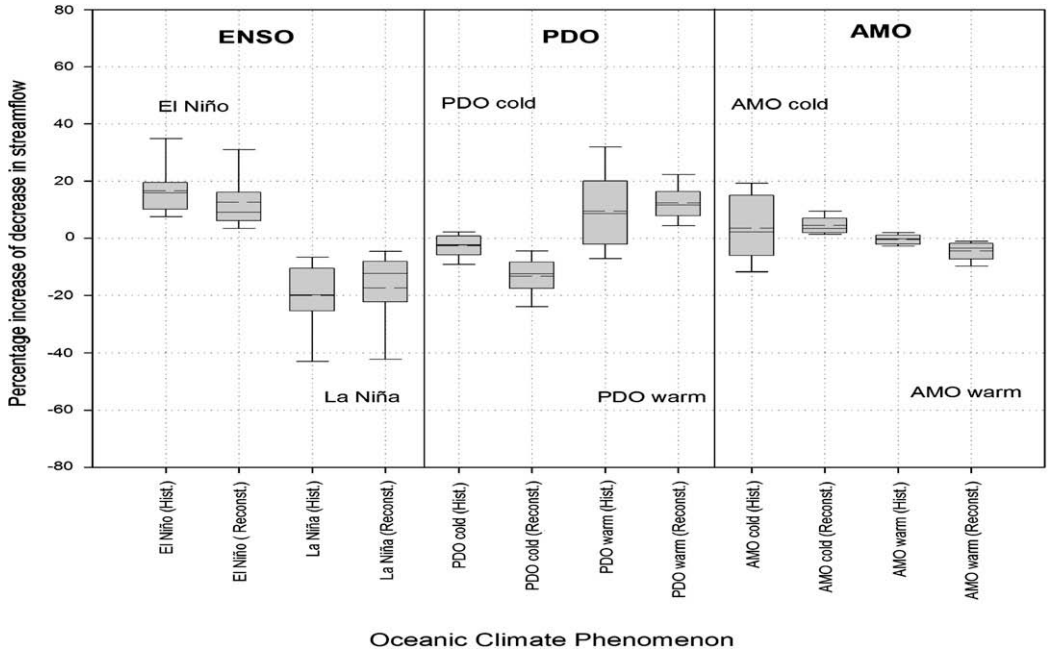

Fig. 5. Box and Whisker plots that shows mean, median, and percentile (5th, 25th, 75th, and 95th) increase/decrease (in terms of percentage) in streamflow volume (considering all 19 stations) due to individual effect of ENSO, PDO, and AMO using historical and reconstructed data respectively. The box delineates the 25th and 75th percentile. The Whiskers are 5th and 95th percentile. The horizontal dash line inside the box indicates mean. The horizontal bold straight line inside the box indicates the median. The long horizontal dot line indicates the line of zero percentage of increase or decrease.

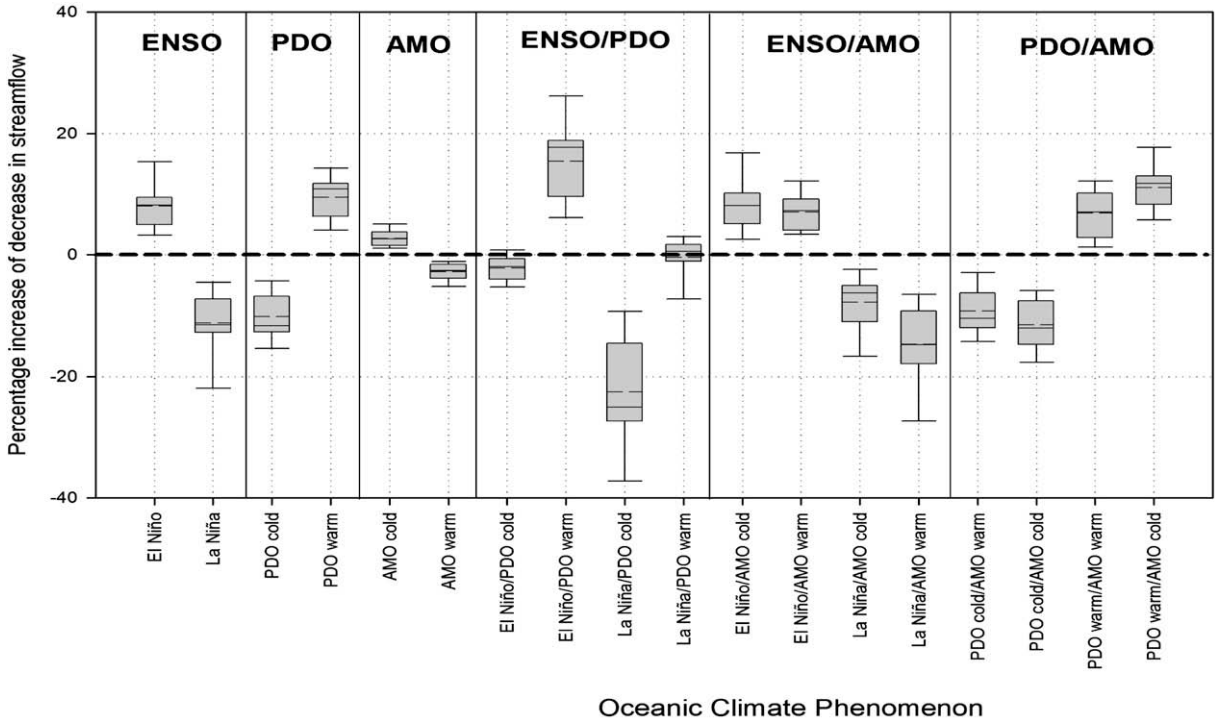

Fig. 6. Box and Whisker plots that shows mean, median, and percentile (5th, 25th, 75th, and 95th) increase/decrease (in terms of percentage) in streamflow volume (considering all 14 stations of upper basin only) due to individual and coupling effect of oceanic climate phenomenon The box delineates the 25th and 75th percentile. The Whiskers are 5th and 95th percentile. The horizontal dash line inside the box indicates mean. The horizontal bold straight line inside the box indicates the median. The long horizontal dot line indicates the line of zero percentage of increase or decrease.

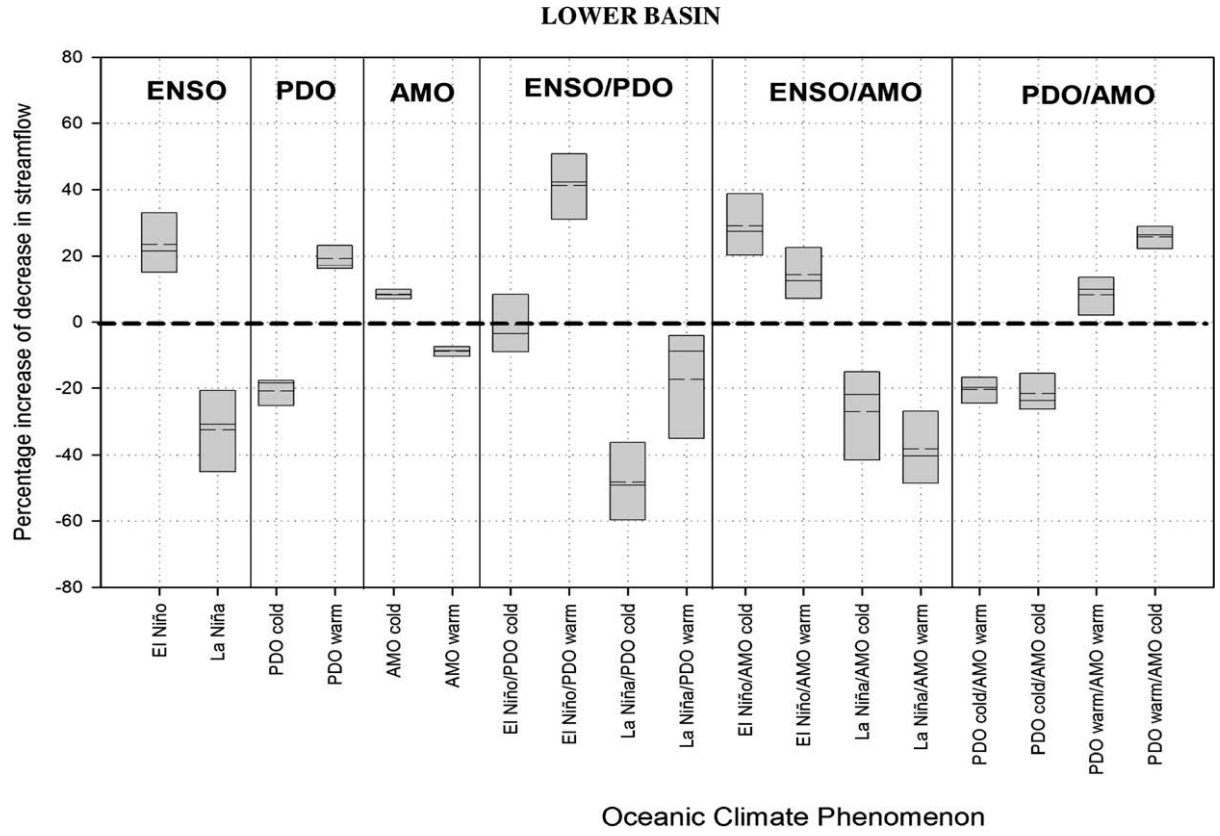

Fig. 7. Box plots showing the mean, median, and percentile (lowest and highest) increase/decrease (in terms of percentage) in streamflow volume (considering all five stations of lower basin only) due to individual and coupling effect of oceanic climate phenomenon. The horizontal dash line inside the box indicates mean. The horizontal bold straight line inside the box indicates the median. The long horizontal dot line indicates the line of zero percentage of increase or decrease.

during ENSO years. The result was similar to that of Enfield et al. (2001) that concluded warm phases of AMO resulted in below normal rainfall in most parts of the United States. Further, PDO warm coupled with AMO cold enhanced the streamflow volume in the basin and this relation was consistent with McCabe et al. (2007).

The impact of using a longer record from reconstructed data as compared to the instrumental record was compared in Fig. 5. The plot shows that the PDO cold and warm had shifts in the mean using reconstructed data that were higher than those seen using instrumental records. The variability of the response was reduced in the reconstructed data of PDO warm and AMO cold, which demonstrates a certain level of persistence in the responses to PDO and AMO during the reconstructed period.

Finally, the mean difference in percentage were separately calculated and plotted for the streamflow stations located for Upper Colorado River Basin (Fig. 6) and Lower Colorado River Basin (Fig. 7), respectively. In the Upper Colorado River basin, there were 12 streamflow stations and these were associated with increased streamflow during the El Niño(ENSO warm), PDO warm, AMO cold, El Niño/PDO warm, El Niño/AMO cold, El Niño/AMO warm, and PDO warm/AMO cold. During the La Niña (ENSO cold), PDO cold, AMO warm, La Niña/PDO cold, La Niña/AMO cold, La Niña/AMO warm, PDO cold/ AMO warm, and PDO cold/ AMO cold there was decreased streamflow. Similar to the result of whole basin (Upper and Lower), El Niño/ La Niña patterns during the positive/negative phase of PDO had the strongest influence on the upper basin streamflow and the maximum increased/decreased streamflow of about 15–25%.

In the Lower Colorado River basin (Fig. 7), the El Niño, PDO warm, AMO cold, El Niño/PDO warm, El Niño/AMO cold, El Niño/AMO warm, PDO warm/AMO warm, and PDO warm/AMO cold had increased streamflow volume. Similarly, La Niña, PDO cold, AMO warm, La Niña/PDO cold, La Niña/PDO warm, La Niña/AMO cold, La Niña/AMO warm, PDO cold/ AMO warm, and PDO cold/ AMO cold had decreased streamflow. In most of the cases, the individual and coupled impact of ocean climate phenomenon had similar effect on the Upper and Lower basin but the magnitude of percentage increase or decrease was higher in the Lower basin. In Lower basin, the El Niño/ La Niña patterns during the positive/negative phase of PDO had the strongest influence on streamflow and had the maximum increased/decreased streamflow of about 40–50%, which was about the double the magnitude of the upper basin.

Conclusions

The research presented here contributes to a better understanding how interannual and interdecadal phenomenon impact streamflow in the Colorado River basin using reconstructed data from 1706 to 1970. The previous research (e.g. Tootle et al., 2005; Hunter et al. 2006; McCabe et al., 2007, and Gershunov and Barnett, 1998) evaluated the individual and coupling effect of ocean climate phenomenon (ENSO, PDO, AMO, and NAO) using an instrumental record of 50–100 years. Using a longer record had similar results in the shift of the median as the instrumental record, but the variability was less using the longer record.

Overall, it was found that there is an increase in streamflow during El Niño and decreased streamflow during La Niña. This is consistent with the previous studies using instrumental data (e.g.: Redmond and Koch, 1991; Piechota and Dracup, 1996, and Cayan et al. 1999). Similarly, the result of increased streamflow in the basin during to the warm phase of PDO was consistent with the result of Tootle et al. (2005) and Hunter et al. (2006) for the southwest. However, this study found a stronger response in streamflow in terms of the number of stations and magnitude as compared to Tootle et al. (2005) and Hunter et al. (2006). Contrary to the McCabe et al. (2007) study, this study identified few significant stations based on Rank Sum test that were associated with AMO. However, the result of a coupled impact during AMO cold and PDO warm resulting in higher streamflow was consistent with McCabe et al. (2007).

While comparing the results based on the mean (percentage increase or decrease) of streamflow stations located in the Upper and Lower basin, it was found that the magnitude of changes in streamflow (in terms of percentage) was higher in the Lower basin as compared to the upper basin.

Acknowledgements

The PI's at the University of Nevada, Las Vegas are supported by the US National Science Foundation award CMS-0239334, the US Bureau of Reclamation, the National Oceanic and Atmospheric Administration under award NA070AR4310228, and the University of Nevada, Las Vegas, Department of Civil and Environmental Engineering. The PI at the University of Tennessee is supported by the Wyoming Water Development Commission, the USGS/State of Wyoming Water Research Program and the University of Wyoming, Office of Water Programs.

References

Abdi, H., 2003. Partial least squares regression. In: Bryman, M.A., Futing, T. (Eds.), Encyclopedia of Social Sciences Research Methods. Lewis-Beck, London, UK.
Ablitt, N.A., Gao, J., Keengan, J., Stegger, L., Firmin, D.N., Yang, G., 2004. Predictive cardiac motion modelling and correction with partial least squares regression. IEEE Transactions on Medical Imaging 23 (10), 1315–1324.
Biondi, F., Gershunov, A., Cayan, D.R., 2001. North Pacific Decadal climate variability since 1661. Journal of Climate 14, 5–10.
Cayan, D.R., Redmond, K.T., Riddle, L.G., 1999. ENSO and hydrologic extremes in the Western United States. American Meteorological Society 12, 2881–2893.
Cook, E.R., Jacoby, G.C., 1983. Potomac River streamflow since 1730 as reconstructed by tree-rings. Journal of Climate and Applied Meteorology 22 (10), 1659–1672.
Cook, E.R., Meko, D.M., Stahle, D.W., Cleaveland, M.K., 1999. Drought reconstructions for the continental United States. Journal of Climate 12, 1145–1162.
Cook, E.R., Woodhouse, C.A., Eakin, C.M., Meko, D.M., Stahle, D.W., 2004. Long-term aridity changes in the Western United States. Science 306 (5698), 1015–1018.
Dettinger, M.D., Diaz, H.F., 2000. Global characteristics of stream flow seasonality and variability. Journal of Hydrometeorology 1, 289–310.
Diaz, S.C., Touchan, R., Swetnam, T.W., 2001. A tree-ring reconstruction of past precipitation for Baja California Sur, Mexico. International Journal of Climatology 21, 1007–1019.
Enfield, D.B., Mestas-Nuñez, A.M., Trimble, P.J., 2001. The Atlantic multidecadal oscillation and its relation to rainfall and river flows in the continental US. Geophysical Research Letters 28 (10), 2077–2080.
Fritts, H.C., 1976. Tree Rings and Climate. Academic Press, London.
Fritts, H.C., 1991. Reconstructing Large-Scale Climatic Patterns from Tree-ring Data. University of Arizona Press, Tucson. pp. 286.
Garen, D.C., 1992. Improved techniques in regression-based streamflow volume forecasting. Journal of Water Resources Planning and Management 118, 654–670.
Geladi, P., Kowalski, B., 1986. Partial least squares regression: a tutorial. Anaytica Chimica Acta 185, 1–17.
Gerlach, R.W., Kowalski, B.R., Wold, H.O.A., 1979. Partial least-squares path modelling with latent variables. Analytica Chimica Acta 112 (4), 417–421.
Gershunov, A., Barnett, T.P., 1998. Interdecadal modulation of ENSO teleconnections. Bulletin of American Meteorological Society 79, 2715–2725.
Gray, S.T., Graumlich, L.J., Betancourt, J.L., Pederson, G.T., 2004. A tree-ring based reconstruction of the Atlantic multidecadal oscillation since 1567 AD. Geophysical Research Letters 31, L12205.
Hanley, D.E., Bourassa, M.A., O'Brien, J.J., Smith, S.R., Spade, E.R., 2003. A quantitative evaluation of ENSO indices a notes and correspondence. American Meteorological Society 16, 1249–1258.
Hidalgo, H.G., Piechota, T.C., Dracup, J.A., 2000. Streamflow reconstruction using alternative PCA-based regression procedures. Water Resources Research 36 (11), 3241–3249.
Hunter, T., Tootle, G.A., Piechota, T.C., 2006. Oceanic–atmospheric variability and western US snowfall. Geophysical Research Letters 33:L13706. doi:10.1029/2006GL026600.
Kalela-Brundin, M., 1999. Climatic information from tree-rings of *Pinus sylvestris L.* and a reconstruction of summer temperatures back to AD 1500 in Femundsmarka, eastern Norway, using partial least squares regression (PLS) analysis. The Holocene 9, 59–77.
Kerr, R.A., 2000. A North Atlantic climate pacemaker for the centuries. Science 288, 1984–1986.
Maidment, D.R., 1993. Handbook of Hydrology. McGraw-Hill, New York, NY.

Malinowski, E., 2002. Factor Analysis in Chemistry, third ed. Wiley and Sons, New York, NY.
Mantua, N.J., Hare, S.R., Zhang, Y., Wallace, J.M., Francis, R.C., 1997. A Pacific decadal climate oscillation with impacts on salmon. Bulletin of the American Meteorological Society 78, 1069–1079.
McCabe, G.J., Betancourt, J.L., Hidalgo, H.G., 2007. Association of decadal to multidecadal variability with Upper Colorado River flow. Journal of American Water Resources Association 43 (1), 183–192.
Meko, D.M., Therrel, M.D., Baisan, C.H., Huges, M.K., 2001. Sacramento River flow reconstructed to AD 869 from tree-rings. Journal of American Water Resources Association 37 (4), 1029–1040.
Michealson, J., 1987. Cross validation in statistical climate forecast models. Journal of Applied Meteorology 26 (11), 1589–1600.
Moberg, A., Sonechkin, D.M., Holmgren, K., Datsenko, N.M., Karlen, W., 2005. Highly variable Northern Hemisphere temperatures reconstructed from low- and high resolution proxy data. Nature 433, 613–617.
Piechota, T.C., Dracup, J.A., 1996. Drought and regional hydrologic variations in the United States: associations with the El Niño/Southern Oscillation. Water Resources Research 32 (5), 1359–1373.
Redmond, K.T., Koch, R.W., 1991. Surface climate and streamflow variability in the western United States and their relationship to large-scale circulation indices. Water Resources Research 27 (9), 2381–2399.
Shen, C., Wang, W.C., Gong, W., Hao, Z., 2006. A Pacific decadal oscillation record since 1470 AD reconstructed from proxy data of summer rainfall over eastern China. Geophysical Research Letters 33, L03702. doi:10.1029/2005GL024804.
Slack, J. R., and J. M. Landwehr, 1993. Hydro-climatic data network: A U.S. geological survey streamflow data set for the United States for the study of climate variations, 1874–1988. USGS Open-File Report 92–129. <http://pubs.usgs.gov/of/1992/ofr92-129/content.html> (accessed 10.07.06).
Stahle, D.W., Cleaveland, M.K., Blanton, D.B., Therrell, M.D., Gay, D.A., 1998a. The lost colony and Jamestown droughts. Science 280, 564–567.
Stahle, D.W., D'Arrigo, R.D., Krusic, P.J., Cleaveland, M.K., Cook, E.R., Allan, R.J., Cole, J.E., Dunbar, R.B., Therrell, M.D., Gay, D.A., Moore, M.D., Stokes, M.A., Burns, B.T., Villanueva-Diaz, J., Thompson, L.G., 1998b. Experimental dendroclimatic reconstruction of the Southern Oscillation. Bulletin of American Meteorological Society 79, 2137–2152.
Stockton, C.W. and G.C. Jacoby, 1976. Long-term Surface Water Supply and Streamflow Trends in the Upper Colorado River Basin. Lake Powell Research Project, Bulletin No. 18, National Science Foundation, p. 70.
Sutton, R.T., Hodson, D.L.R., 2005. Atlantic Ocean forcing of north American and European summer climate. Science 309, 115–118.
The ENSO cycle: Southern Oscillation Index (SOI), 2006. Pacific ENSO update, National Oceanic and Atmospheric Administration, 12(1), 11.
Timilsena, J., Piechota, T.C., Hidalgo, H.G., Tootle, G., 2007. Five hundreds years of drought in the Upper Colorado River basin. Journal of American Water Resources Association 43 (3), 798–812.
Tootle, G.A., Singh, A.K., Piechota, T.C., Farnham, I., 2007. Long lead time forecasting of U.S. streamflow using partial least squares regression. Journal of Hydrologic Engineering 12 (5), 442.
Tootle, G.A., Piechota, T.C., Singh, A.K., 2005. Coupled oceanic-atmospheric variability and US streamflow. Water Resources Research 41, W12408.
Touchan, R., Meko, D.M., Huges, M.K., 1999. A 396-year reconstruction of precipitation in southern Jordan. Journal of the American Water Resources Association 35 (1), 49–59.
Wold, H., 1966. Estimation of principal components and related models by iterative least squares. In: Krishnaiah, P.R. (Ed.), Multivariate Analysis. Academic Press, New York, pp. 391–420.
Wold, S., Geladi, P., Esbensen, K., Ohman, J., 1987. Multi-way principal components and PLS analysis. Journal of Chemometrics 1, 41–56.
Woodhouse, C.A., 2001. A tree-ring reconstruction of streamflow for the colorado front range. Journal of the American Water Resources Association 37, 561–569.
Woodhouse, C.A., Gray, S.T., Meko, D.M., 2006. Updated streamflow reconstructions for the Upper Colorado River basin. Water Resources Research 42. W05415.